Fuel 372 (2024) 132256

Contents lists available at ScienceDirect

Fuel

journal homepage: www.elsevier.com/locate/fuel

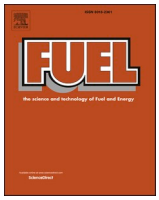

Full Length Article

Hydrochar from winemaking industry wastes as solid biofuel: A thermal and kinetic analysis of pyrolysis and combustion

Alessandro Cardarelli, Marco Barbanera *

Department of Economics Engineering Society and Business Organization (DEIM), University of Tuscia, Largo Dell'Università S.n.c., Loc. Riello, 01100 Viterbo, Italy

ARTICLE INFO

Keywords:
Hydrothermal carbonization
Kinetics
Thermodynamic analysis
Thermogravimetry
Winemaking industry wastes

ABSTRACT

Pyrolysis and combustion behavior of the hydrochar (HY) from co-hydrothermal carbonization (co-HTC) of vine pruning (VP) and exhausted grape marc (EGM) by using vinasse as wet catalytic vector was investigated through thermogravimetric analysis (TGA). For both raw- and co-HTC biomass, different *iso*-conversional methods were used for kinetic analysis, and the thermodynamic parameters were determined. Overall, even if HY exhibited a lower activation energy compared to EGM and VP during both pyrolysis and combustion, HTC has positive effects on the hydrochar's structure, which achieved a more thermodynamically stable, structurally ordered, and energetically favorable state. The obtained kinetic and thermodynamic parameters would contribute to the development of biomass thermochemical conversion technologies and the application of hydrochar-based energy systems.

1. Introduction

In 2020 the European Union (EU) surpassed its 20 % target of gross final energy consumption from renewable sources, as outlined in the 2009 Renewable Energy Directive (RED I), by achieving a 22 % share [1]. The recent agreement between the European Parliament and the Council in the recast RED II (2018/2001/EU) introduced a new strengthening renewable energy target of at least 42.5 % share by 2030 (RED III) [2,3]. This means almost doubling the current share of renewable energy sources (RES) in the EU. RES achieved their highest level of integration in the power sector, accounting for 37.5 % of the total electricity generated in the EU in 2021. Subsequently, the heating and cooling sector followed with a RES share of 22.9 % while in transport contributed to 9.1 % of the overall share [4]. Solid biomass stands out as the most prominent renewable energy source, dominating the renewable energy supply in Europe [5,6]. It finds extensive application in heating and industrial sectors, accounting for a substantial 41 % share in 2021. Following behind are wind energy (13 %), hydropower (12 %), liquid biofuels (8 %), and biogas (6 %), while heat pumps and solar photovoltaics represent less than 6 % individually. With its great potential to boost the EU to get on track with the 2030 agenda, bioenergy from biomass has become of central role in the clean energy transition.

Vine pruning (VP) residue, exhausted grape marc (EGM), and vinasse are waste by-products generated by the winery and distillery industry. These by-products have the potential to be used as feedstocks for the production of biofuels. The conversion of these biomasses into biofuels represents an opportunity to reduce waste, contribute to sustainable energy production, and promote a circular economy approach while also addressing environmental concerns. In the European Union, around 26.4 million tonnes of fresh grapes in 2022 were produced, about 25 % of which remained as waste marc [7,8]. The latter could generate up to 525 million liters of ethanol and thus around 6,565 million liters of vinasse as a residue of the distillation process [9–12]. The economic and environmental challenges associated with the proper management of winery waste pose a significant concern. However, the primary obstacle in utilizing winery and distillery waste lies in their high moisture levels, causing great transportation expenses and increased energy consumption for the necessary drying before their utilization [13]. The hydrothermal carbonization (HTC) process has been largely evaluated as a valuable option to convert wet biomasses into solid biofuels (hydrochars) with upgraded chemical-physical characteristics. Unlike pyrolysis, gasification, torrefaction, and incineration, HTC can efficiently handle wet feedstocks without previous dewatering since water works as a reactant, solvent, and catalyst [14–17].

Our previous work successfully demonstrated the effectiveness of the HTC process on the production of hydrochar (HY) from the co-hydrothermal carbonization of VP and EGM by using vinasse as moisture source [18]. A high-quality hydrochar and an enriched spent liquor

* Corresponding author.
E-mail address: m.barbanera@unitus.it (M. Barbanera).

https://doi.org/10.1016/j.fuel.2024.132256
Received 29 February 2024; Received in revised form 8 June 2024; Accepted 14 June 2024

residue with bioactive compounds were obtained at the optimal HTC operational conditions (temperature, residence time, and biomass-to-liquid ratio) while minimizing the energy consumption of the entire process. The findings demonstrated a circular and sustainable strategy for waste management in the winery and distillery industry.

The great potential of hydrochars as an alternative to fossil fuels due to their high carbon content, calorific value, increased hydrophobicity and grindability (which means reduced problems for storage and transport), and carbon neutral potential has been largely evaluated. Prasongthum et al. [19] investigated the production of hydrochar from oil palm trunks, resulting in lower slagging and fouling issues during combustion in comparison to raw biomass. Sattasathuchana et al. [20] found that the utilization of hydrochar from co-HTC of palm kernel shell and bamboo to produce electricity in a municipal power plant could reduce the fuel storage size by 34 %, save around 28,000 USD/year of transportation cost and reduce 2300 ton/year of CO_2 emissions during burning in comparison of raw biomass. Yu et al. [21] explained that the combination of HTC and pelletization on Ginkgo leaf residues is an efficient technique to produce a solid biofuel with upgraded characteristics. Also, Wu et al. demonstrated that the co-hydrothermal carbonization synergy of food waste and corn stover is beneficial for the physicochemical properties and combustion performance of the resulting hydrochar [22]. Furthermore, the HTC process was demonstrated to be a valuable environmental solution to produce hydrochar as a substitute for fossil coal for metallurgical applications [23]. Although prior studies have investigated the pyrolysis and combustion characteristics of hydrochar from various biomass sources, the unique properties of both raw- and co-hydrothermal carbonized biomass from winery and distillery residues have not been extensively studied. This work provides novel insights by conducting detailed thermal and kinetic analyses of the pyrolysis and combustion behavior of hydrochar from co-hydrothermal carbonization of vine pruning and exhausted grape marc by using vinasse as wet catalytic vector.

Model-free *iso*-conversional methods have been used for studying the decomposition kinetics by using data obtained from thermal gravimetric analysis (TGA) [24–26]. The kinetic parameters, i.e. activation energy (E_a), pre-exponential factor (A), and reaction mechanism (f(α)), collectively known as 'kinetic triplet', and thermodynamic parameters, enthalpy (ΔH), Gibbs free energy (ΔG), and entropy (ΔS) were determined. Understanding and optimizing the design and performance of reactors and energy systems requires a deep comprehension of the temperature at which biomass breaks down. This study provides valuable insights into the mechanisms, rates, and factors involved in the pyrolysis and combustion of winery and distillery by-products and hydrochar. By gaining this comprehensive knowledge, it becomes possible to develop sustainable and effective biomass use techniques, as well as advance the field of hydrochar-based renewable energy [27]. Furthermore, incorporating kinetic information within computational fluid dynamics, would guide the design and optimization of large-scale reactors, determine residence times, and assess mass and heat transfer efficiencies. This aids in the efficient and cost-effective development of industrial processes.

Finally, building upon our previous work aimed at finding an alternative strategy to manage the waste generated by the winemaking industry [18], this research addresses an important gap in the circular bioeconomy. The comprehensive investigations of the pyrolysis and combustion behaviors of the winemaking waste-derived hydrochar provide novel data that expands the limited existing knowledge on this feedstock, representing an opportunity to enhance the sustainability of the winery and distillery industry.

2. Materials and methods

2.1. Preparation and analysis of samples

A local farm in Umbria, located in the center of Italy, provided the vine pruning residue while Bonollo distillery (Italy) the exhausted grape marc and vinasse. The optimum HTC process parameter for hydrochar production, corresponding to a reaction temperature of 246.3 °C, a residence time of 1.6 h and a solid-to-liquid ratio of 0.066 with a 50 wt% raw biomasses blend respectively of VP and EGM, were determined in our previous work [18]. Data about ultimate analysis, proximate analysis, compositional analysis, and Lower Heating Value (LHV) of the raw biomasses and the hydrochar can be found in our previous study [18].

2.2. TG analysis under N_2 and air

The pyrolysis and combustion behavior of the samples were evaluated from the thermogravimetric curves obtained on the Leco TGA-701 analyzer (LECO Corporation, St. Joseph, MI, USA). The samples were heated from room temperature (about 25 °C) to 800 °C at four different heating rates (10, 20, 30, and 40 °C/min), assuming that complete degradation of the sample is achieved at this temperature. Two gas atmospheres of nitrogen (N_2) and air (21 % O_2/79 % N_2) were used respectively to simulate pyrolysis and combustion conditions with a gas flow rate of 50 mL/min. To ensure reliable results, each test was replicated three times, and the averages were calculated to account for experimental reproducibility, which fell within the range of ± 3 %. During each test, a blank run was performed using an empty pan to compensate for buoyancy effects. The weight loss (TG) curves and their respective first-order derivatives (differential thermogravimetric (DTG)) were recorded over time and temperature. Several parameters were directly computed by analyzing the results to identify the main pyrolysis and combustion characteristics, i.e. the initial temperature (T_i), the final temperature (T_f), and the peak temperature (T_p). T_i represents the temperature at which a conversion of 1 % of the initial mass is obtained after the initial weight loss caused by the moisture. T_f is the temperature at which the degradation is almost complete and was defined as the temperature at which the conversion rate reaches 1 %/min at the end of the DTG curve. The fuel reactivity was considered by accounting T_p which corresponds to the temperature of the maximum weight loss rate. Lower reactivity is determined by higher peak temperature [28].

2.3. Kinetic, reaction mechanism, and thermodynamic analysis

The kinetics analysis of the raw biomasses and hydrochar pyrolysis and combustion was evaluated by the integral *iso*-conversional methods of Starink (STK) [29], Kissinger-Akahira-Sunose (KAS) [30], and Ozawa-Flynn-Wall (OFW) [31,32]. According to the Arrhenius equation, the general equation of reaction rate can be expressed by Eq. (1):

$$\frac{d\alpha}{dt} = k(T)f(\alpha) = Ae^{-(E_a/RT)}f(\alpha) \tag{1}$$

where t is the time, T is the absolute temperature (K), A is the pre-exponential factor (s^{-1}), E_a is the apparent activation energy (kJ/mol), and R is the gas constant (8.314 J/mol K), and f(α) is the reaction mechanism.

The conversion degree α during the reaction of the sample can be defined as:

$$\alpha = \frac{m_0 - m_t}{m_0 - m_f} \tag{2}$$

where m_0 and m_f represent the initial and final weights of the sample respectively, and m_t represents the weight of the sample at time t.

Rearranging Eq. (1) by introducing the constant heating rate $\beta = dT/dt$ the differential form of the non-isothermal rate law becomes:

$$\frac{d\alpha}{dT} = \frac{A}{\beta}e^{-(E_a/RT)}f(\alpha) \tag{3}$$

Since the differential form exhibits low accuracy, leading to scattered derivative curves, the integral form of Eq. (3) is usually more suitable for

determining activation energy values [33,34], which brings to Eq. (4):

$$g(\alpha) = \int_0^{\alpha} \frac{d\alpha}{f(\alpha)} = \frac{A}{\beta}\int_{T_0}^{T} e^{-(E_a/RT)}dT \quad (4)$$

As the integral form (Eq. (4)) does not have an analytical solution, the approximate solutions of STK (Eq. (5)), OFW (Eq. (6)), and KAS (Eq. (7)) were considered to determine the kinetic parameters, since *iso*-conversional methods can obtain reliable kinetics parameters by using multiple heating rates without requiring the reaction model [33].

$$ln\left(\frac{\beta}{T^{1.92}}\right) = -1.0008\frac{E_a}{RT} + Const \quad (5)$$

$$ln(\beta) = ln\left(\frac{AE_a}{Rg(\alpha)}\right) - 5.331 - 1.052\frac{E_a}{RT} \quad (6)$$

$$ln\left(\frac{\beta}{T^2}\right) = ln\left(\frac{AR}{E_a g(\alpha)}\right) - \frac{E_a}{RT} \quad (7)$$

For the STK method, the activation energy can be obtained from the slope of the fitted straight line by plotting $\ln(\beta/T^{1.92})$ vs. 1/T at the given conversion degree α. Similarly, by using the OFW method, based on Doyle's approximation [35,36], a linear relationship is established by plotting ln(β) against 1/T and the resulting slope is equal to $-1.052E_a/R$. Lastly, from the KAS method, the value of E_a can be determined from the slope of the fitted straight line formed by using $\ln(\beta/T^2)$ vs. 1/T.

While *iso*-conversional methods are highly accurate in determining E_a values, they do not provide information about the pre-exponential factor. Thus, the energy compensation effect (ECE) method was used to estimate the values of A. By taking the logarithm on both sides of Eq. (3) and rearranging the terms, ln A_i and $E_{a,i}$ can be calculated from the intercept and the slope of the regression lines by plotting $\ln[\beta(d\alpha/dT)/f_i(\alpha)]$ vs. 1/T, where i refers to the mechanism function listed in Tab. SI 1. The linear relationship between $E_{a,i}$ and ln A_i, known as the compensation effect and described by Eq. (8), allows to find the compensation parameters a and b [37].

$$lnA_i = aE_{a,i} + b \quad (8)$$

Once the compensation parameters are determined, the values of A are obtained with Eq. (8) by using the E_a values beforehand determined by an *iso*-conversional method.

To complete the kinetic triplet is essential to determine the decomposition mechanism, which could be predicted by the master-plot method. By approximating to zero the lower limit (T_0) of the integral on the right side of Eq. (4), as the rate of decomposition is extremely slow at ambient temperature [38,39], the mentioned equation can be rewritten in Eq. (9):

$$g(\alpha) = \frac{AE_a}{\beta R}p(u) \quad (9)$$

where $p(u) = \int_{\infty}^{u} -\left(\frac{e^{-u}}{u^2}\right)du$ is the temperature integral and u = E_a/RT. p(u) has no analytical solution and can be expressed by numerical approximation as Doyle's (Eq. (10)), which gives sufficiently reliable results [40].

$$p(u) = 0.0048e^{-1.0516u} \quad (10)$$

Using a reference at point α = 0.5 and according to Eq. (9), Eq. (11) is obtained:

$$\frac{g(\alpha)}{g(0.5)} = \frac{p(u)}{p(u_{0.5})} \quad (11)$$

Thus, the experimental curves plotted as $p(u)/p(u_{0.5})$ for a given α, using data obtained at various heating rates, and the theoretical master plot represented as g(α)/g(0.5) are comparable when an appropriate kinetic model is employed.

Establishing thermodynamic parameters such as changes in enthalpy (ΔH), Gibbs free energy (ΔG), and entropy (ΔS) is a prerequisite for scaling up a process to industrial level, as it enables accurate energy calculations [41,42]. These parameters were evaluated using kinetic data (E_a and A) and thermogravimetric data points according to Eq. (12), (13), and (14), where k_B is the Boltzmann constant (1.381×10^{-23} J/K), and h is the Plank constant (6.626×10^{-34} J/s).

$$\Delta H = E_a - RT \quad (12)$$

$$\Delta G = E_a + RT_p ln\left(\frac{k_b T_p}{hA}\right) \quad (13)$$

$$\Delta S = \frac{\Delta H - \Delta G}{T_p} \quad (14)$$

3. Results and discussion

3.1. Pyrolysis behavior

The thermal degradation profiles of VP, EGM, and HY under a nitrogen atmosphere at a 10 °C/min heating rate are shown in Fig. 1. The TG and DTG profiles at 20, 30, and 40 °C/min are displayed in the Supplementary material (Figure S1) since no significant differences were revealed. All the DTG (%/min) curves present the dehydration stage in which weakly bonded water molecules are released between 50 – 150 °C. Then, the devolatilization and the decomposition of the major components of the biomass, i.e. hemicellulose, cellulose, and lignin, occur [43]. While EGM exhibited two main stages between 154 – 291 °C (stage I) and 291 – 649 °C (stage II), VP showed a single decomposition stage (123 – 657 °C). Compared to the EGM, VP exhibited high mass loss, which might be due to the lower ash and higher volatile content [18]. On the other hand, the area under the decomposition curve of HY considerably decreased in comparison with VP and EGM. Throughout the HTC process, water removes a portion of the loosely bonded amorphous cellulose, hemicellulose, and lignin, along with other water-soluble extractives and intermediate products [44]. As a result, the solid hydrochar is comprised of tightly bonded cellulose, hemicellulose, and lignin formed through recondensation reactions [45]. Consequently, the weight loss experienced by HY is lower compared to the VP

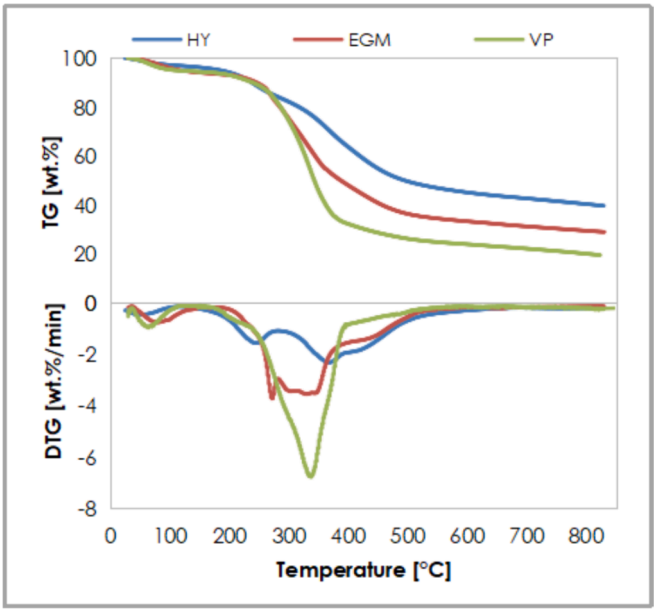

Fig. 1. Thermal degradation profiles of HY, EGM, and VP under N_2 atmosphere with a heating rate of 10 °C/min.

and EGM. Interestingly, the HY displays a lack of decomposition peak within 280 – 360 °C suggesting that hydrothermal treatment caused the degradation of cellulose besides hemicellulose, fats, and proteins [46]. While the second degradation stage between 310 and 728 °C (stage II) could be associated mainly with the degradation of lignin, the first one (stage I) between 114 – 310 °C may be related to the degradation of repolymerized products, which formed during the HTC process [47,48].

3.1.1. *Effect of heating rate*

From the TG and DTG results reported in Fig. 2 and Table 1, it is remarkable that the heating rate affects the conversion and product distribution for each sample and results in an important parameter in possible commercial applications in determining the type of reactor to be used [49,50]. When the samples are heated at higher β a slight shift is observed and the peak temperature of weight loss increases. This phenomenon, referred to as heat transfer limitation, caused the observed thermal lag. As the heating rate increases, the temperature gradient between the interior and exterior of the particles also increases. This leads to a lower degree of reaction occurring inside the particles compared to the outside, requiring higher temperatures to decompose the material [39,51]. In contrast, when lower heating rates are employed, the particles experience a gradual and more efficient heat transfer towards the inner portions and among the particles [52,53]. As a result, the peak of the weight loss rate shifts towards lower values. Furthermore, by considering the temperature of initial (T_i) and final (T_f) degradation, the pyrolysis of HY took place over a broader temperature range, spanning from 181 to 657 °C, in comparison to VP, 186 – 565 °C, and EGM, 181 – 571 °C. Notably, the T_p significantly resulted higher for HY than raw biomass for each heating rate (Table 1), and the residue rate, by considering β = 10 °C/min as a reference, rose from 19 % of VP and 29 % of EGM to 40 % (Fig. 2). These findings indicate that the feedstock exhibited improved thermal stability after undergoing hydrothermal carbonization [54].

Additionally, to assess the release performance of volatile compo-

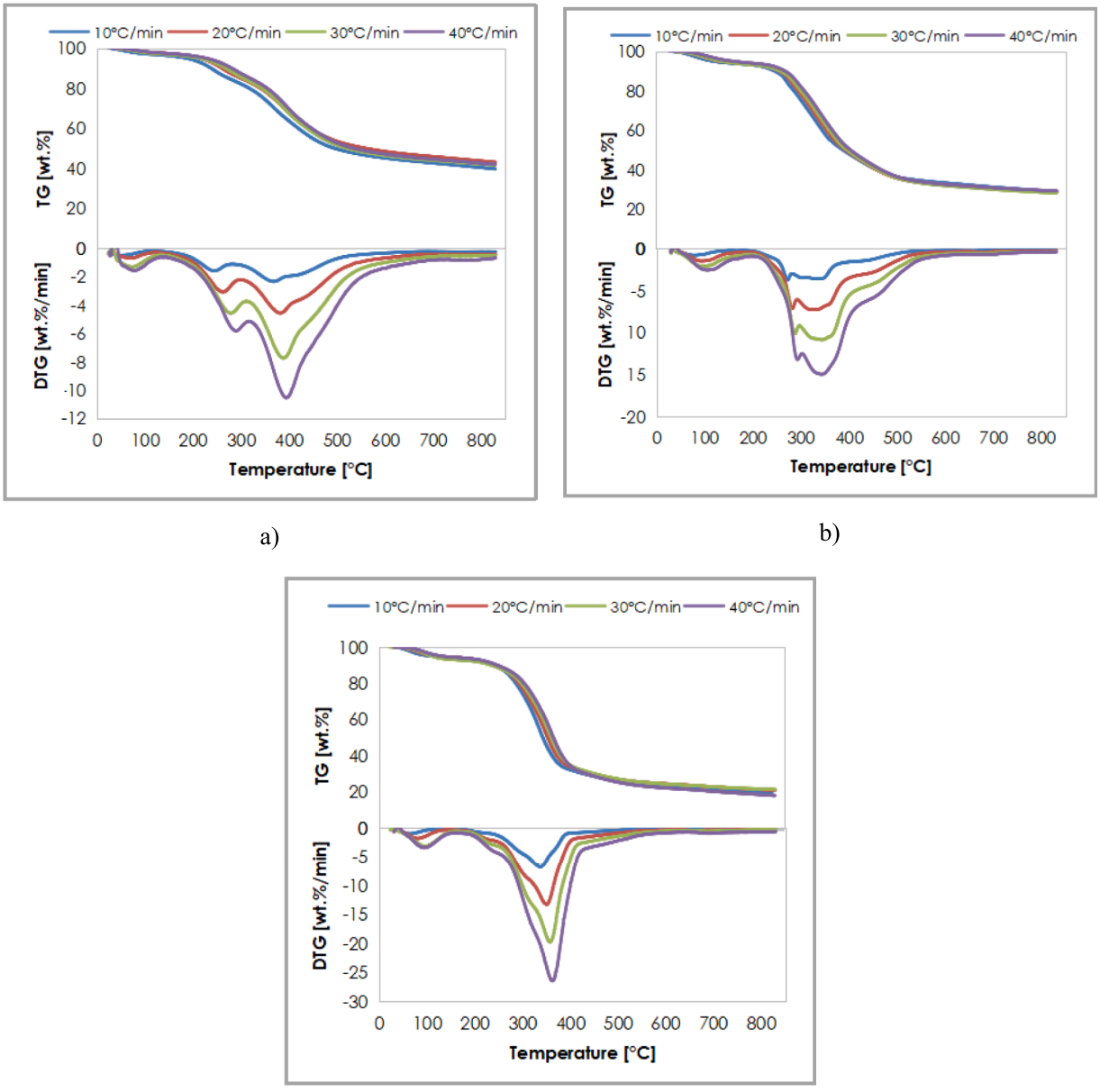

Fig. 2. TG and DTG profiles of (a) HY, (b) EGM, and (c) VP under the N_2 atmosphere at each heating rate.

Table 1
Pyrolysis parameters of HY, EGM, and VP at each heating rate.

β	T_i	T_f	T_p	$-DTG_{max}$	$-DTG_{mean}$	D_i
[°C/min]	[°C]	[°C]	[°C]	[%/min]	[%/min]	[10^{-6} %min^{-1}°C^{-3}]
HY						
10	213.54	476.66	367.27	2.33	2.61	0.12
20	200.80	542.01	381.16	4.56	4.62	0.25
30	189.13	597.54	387.69	7.75	6.22	0.52
40	180.70	657.33	393.52	10.55	7.40	1.58
EGM						
10	236.87	466.60	272.06	3.74	3.18	0.50
20	223.57	516.13	319.87	7.24	5.54	0.78
30	217.42	545.15	343.14	10.86	7.55	1.11
40	181.48	570.60	342.94	14.98	8.88	2.46
VP						
10	237.44	391.41	336.61	6.78	3.57	0.97
20	200.25	482.11	349.79	13.30	5.80	2.23
30	198.68	526.55	357.41	19.79	7.24	3.31
40	185.90	565.20	362.09	26.52	9.29	4.50

nents during the pyrolysis process, the devolatilization index (D_i) was determined according to Eq. (15) [55], where DTG_{max} is the maximum weight loss rate and $\Delta T_{1/2}$ is the temperature range when the value of DTG/DTG_{max} is 1/2. Achieving a larger devolatilization index leads to higher yields of volatile products, making the devolatilization process easier.

$$D_i = \frac{DTG_{max}}{T_i T_p \Delta T_{1/2}} \quad (15)$$

From the results listed in Table 1, the D_i of VP resulted higher than those of EGM for each heating rate. This could be related to the higher content of hemicellulose and cellulose in VP which are more reactive and easier to devolatilize. Nevertheless, compared to its precursors, the devolatilization index of HY at each β was considerably lower, indicating that HTC can increase the content of more thermal stable compounds such as lignin while reducing volatile matter, hemicellulose, extractives, and part of the cellulose. Thus, the HTC promotes the thermal stability of the hydrochar [56,57]. Furthermore, for all the materials D_i increased as the heating rate increased, indicating the devolatilization performance was improved 13 times for HY, and 5 times for EGM and VP as β went up from 10 to 40 °C/min.

3.2. Combustion behavior

The TG and DTG results of hydrochar and its biomass precursors under the air environment are displayed in Fig. 3 performed at a heating rate of 10 °C/min. The results for β equal to 20, 30, and 40 °C/min are available in the Supplementary material (Figure S2) since no noteworthy differences were appreciated. Overall, the mass loss curves for HY, EGM, and VP during combustion resulted in similar trends although with significant differences. The observed profiles align with the combustion patterns commonly observed for biomass fuels, mainly characterized by dehydration, devolatilization, and char oxidation stages [58,59]. For all the samples, the initial mass loss between room temperature and around 130 °C was due to moisture evaporation. Following, the devolatilization stage (stage I) occurred between 157 – 377 °C and 156 – 377 °C for EGM and VP, respectively. Then, the combustion of fixed carbon (stage II), related to the decomposition of lignin, emerged between 377 – 708 °C for EGM, and 377 – 650 °C for VP [60]. Co-HTC remarkably changed the combustion behavior. For the HY, stage I (135 – 374 °C) was particularly weakened, whereas stage II (374 – 830 °C), i. e. the char oxidation, leaned to be plentiful. These results suggest that the HTC process is an effective thermal treatment aimed at reducing volatile compounds while increasing fixed carbon [61–63].

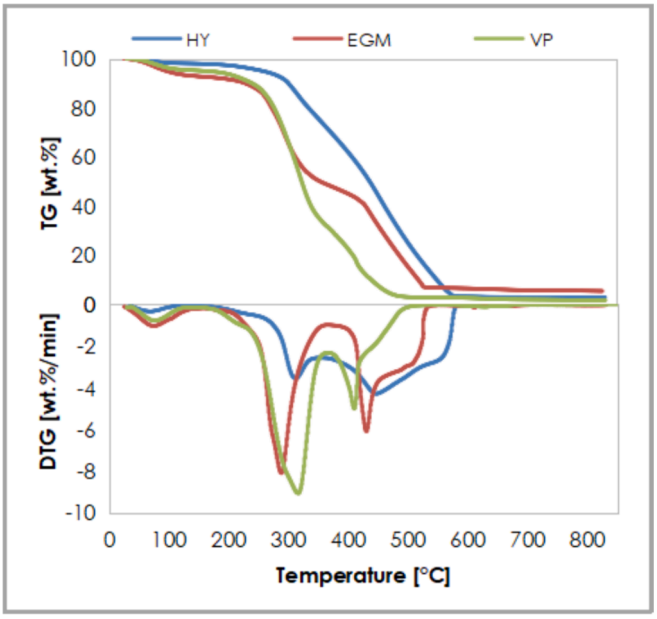

Fig. 3. Thermal degradation profiles of HY, EGM, and VP under air atmosphere with a heating rate of 10 °C/min.

3.2.1. Effect of heating rate

Fig. 4 presents the combustion TG-DTG profiles of all samples at different heating rates, while Table 2 the combustion parameters. For each heating rate, the raw biomasses presented relatively lower T_i compared to HY. The lower content of thermally unstable VM, which releases the heat earlier and reduces the ignition temperature, makes the HY safer during handling, storage, and transportation operations [64]. The impact of increasing the heating rate was limited to causing a shift of the TG and DTG profiles to higher temperature ranges, while having only a minor effect on their overall patterns, primarily due to the influence of heat transfer limitations [65]. However, it is interesting to note that, for EGM and HY, the slower heating rate (10 °C/min) allows for better access of oxygen to the char particles, facilitating the oxidation process and providing more time for the reactions to take place. In this case, the slower heating rate promotes more complete oxidation of the char, resulting in a higher mass loss rate during the char oxidation stage. On the other hand, increasing the heating rate can cause the volatiles to be rapidly released before sufficient oxygen is available for their combustion. As a result, a larger proportion of the mass loss occurs during the devolatilization stage, rather than during the subsequent char oxidation stage [66].

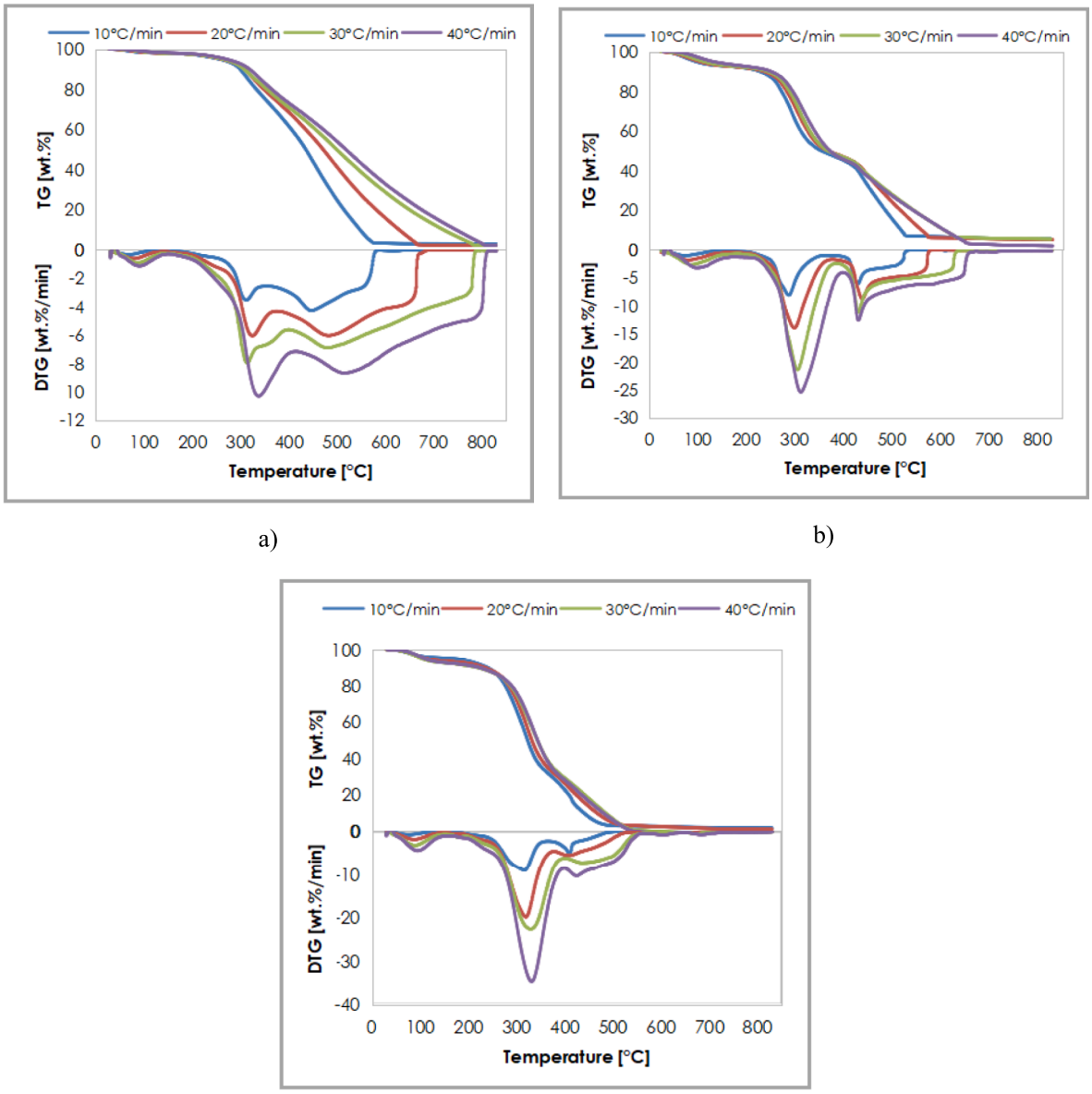

Fig. 4. TG and DTG profiles of (a) HY, (b) EGM, and (c) VP under air atmosphere at each heating rate.

Table 2
Combustion parameters of HY, EGM, and VP at each heating rate.

β	T_i	T_f	T_p	$-DTG_{max}$	$-DTG_{mean}$	S
[°C/min]	[°C]	[°C]	[°C]	[%/min]	[%/min]	[10^{-7} $\%^2min^{-2}°C^{-3}$]
HY						
10	274.65	573.60	446.62	4.29	3.10	3.07
20	237.41	665.76	324.40	6.06	4.47	7.22
30	222.49	782.80	313.24	7.97	5.17	10.64
40	216.36	799.68	337.77	10.31	6.59	18.15
EGM						
10	227.20	519.65	436.23	7.48	3.04	8.48
20	220.00	618.42	299.28	14.67	4.56	22.34
30	215.32	629.77	305.36	21.43	6.51	47.82
40	171.79	655.36	312.07	25.43	7.61	100.05
VP						
10	220.29	469.05	315.82	9.07	3.57	14.24
20	202.06	510.31	319.43	19.90	5.80	55.39
30	170.38	541.42	329.34	22.65	7.24	104.31
40	161.98	548.57	331.59	34.71	9.29	223.97

After co-HTC, HY had higher FC and lower ash and volatile contents compared to EGM and VP, resulting in higher T_f. A higher burnout temperature indicates that the combustion process has been more thorough and complete. It implies that a larger proportion of the fuel has been combusted, resulting in improved combustion efficiency. This is desirable as it maximizes the utilization of the energy content and reduces slagging and fouling tendency during combustion, leading to higher energy conversion [67].

These findings were confirmed by the combustion index (S) calculated according to Eq. (16) [68], where DTG_{mean} is the average

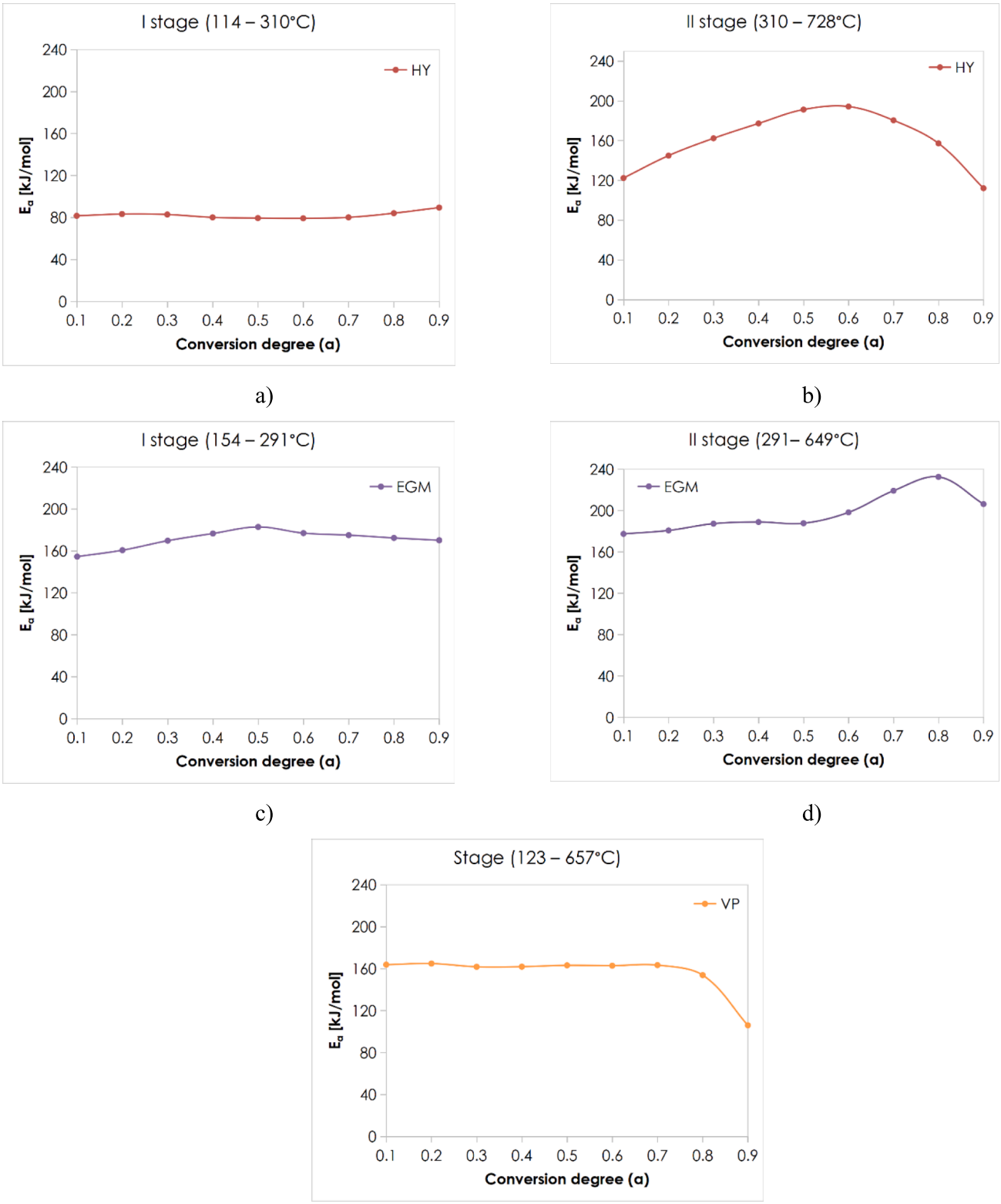

Fig. 5. Trend of apparent activation energy of HY a – b, EGM c – d, and VP e, during pyrolysis obtained by STK method.

conversion rate between ignition (T_i) and burnout temperatures (T_f) [42]. The higher value of S represents better combustion performance as the material is easier to ignite [69].

$$S = \frac{DTG_{max} DTG_{mean}}{T_i^2 T_f} \quad (16)$$

Overall, the combustion index of HY for each heating rate was lower than that of EGM and VP. S at 10 °C/min was respectively 3.07×10^{-7}, 8.48×10^{-7}, and 14.24×10^{-7} $\%^2 min^{-2} {}^{\circ}C^{-3}$. The difference in S between the co-hydrothermal carbonized hydrochar and the raw biomasses increased with the heating rate, reaching respectively 18.15×10^{-7}, 100.05×10^{-7}, and 223.97×10^{-7} $\%^2 min^{-2} {}^{\circ}C^{-3}$ at 40 °C/min for HY, EGM, and VP.

HY showed a lower flammability compared to the original biomass material. The hydrothermal treatment may have induced structural changes in the biomass, resulting in the formation of a more condensed

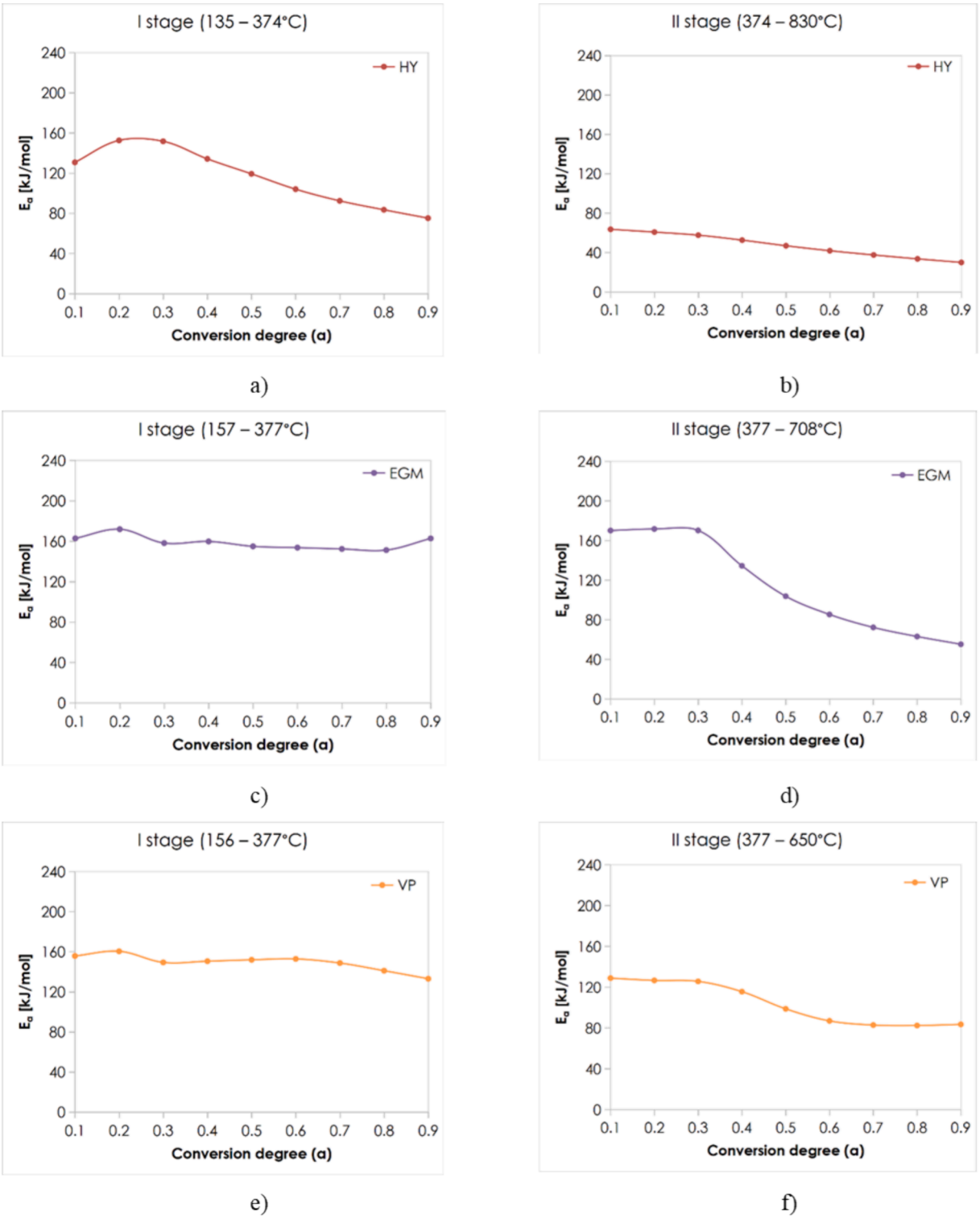

Fig. 6. Trend of apparent activation energy of HY a – b, EGM c – d, and VP e – f, during combustion obtained by STK method.

and stable carbonaceous structure in the hydrochar. Also, it was found that an unstable flame and large heat loss may result during the combustion of solid fuel with high VM content [25,70]. Hence, although EGM and VP exhibited higher S values, their combustion performance may still be inadequate. In contrast, HY, characterized by lower VM and high FC content, might grant a combustion process that is less turbulent and features a more stable flame. The decrease in the combustion index for HY can have both advantages and disadvantages depending on the application. While it may reduce the risk of uncontrolled combustion and self-heating, making it safer to handle, store, and transport, it may also impact the energy density of the material in certain applications, such as energy production or biofuel utilization [71–73]. However, lower combustion properties might be advantageous if used as a solid fuel or carbon source in steelmaking processes, e.g. electric arc furnace (EAF), as a substitute for fossil coal [74,75]. The reduced combustibility ensures the hydrochar may sustain the required high temperatures in the furnace without burning too quickly or uncontrollably. It provides a stable carbon feedstock for the metallurgic process, contributing to efficient and controlled heat generation and carbon dissolution [23,76].

3.3. Kinetic parameters analysis

The kinetic study of pyrolysis and combustion is of great significance to fully assess the behaviors of the samples. As previously discussed in sections 3.1 and 3.2, the main pyrolysis and combustion region of both the raw biomasses and the hydrochar exhibited distinct weight loss stages. To evaluate the kinetic accurately, the kinetic triplets were obtained by stages.

3.3.1. Activation energy

Fig. 5 and Fig. 6 present the changes in the apparent activation energies at each conversion degree obtained with the STK method during pyrolysis and combustion, respectively. No significant differences in E_a values between the *iso*-conversional methods were appreciated. The numerical results from the STK, OFW, and KAS methods, regarding both atmospheres, were reported in the supplementary material (Table S2 – S7). According to Table S2 – S7, the coefficient of determination (R^2) was above 0.9 for all the samples indicating that the apparent activation energy obtained for α between 0.1 and 0.9 had a high degree of consistency. Also, the fitting results based on the *iso*-conversional methods from the pyrolysis and combustion tests are displayed in Figure S3 and Figure S4, respectively. As shown in Fig. 5, in the full pyrolysis decomposition stage of VP and the first stage of HY and EGM, the apparent activation energy did not change significantly with α, mainly because of the rapid degradation of weakly bonded amorphous cellulose and hemicellulose. In the second stage, as α increased, the activation energy of HY and EGM gradually rose until reaching a certain limit and then decreased. Once the weak bonds were degraded, the degradation of all-crystalline cellulose began, with lignin contributing to a further increase in activation energy [77]. Furthermore, regarding the average activation energy values, HY exhibited a lower value (82 kJ/mol) compared with EGM (171 kJ/mol) and VP (156 kJ/mol), in the first stage of pyrolysis. In the second stage, E_a of HY increased up to 160 kJ/mol, remaining lower than EGM (197 kJ/mol) and slightly higher than VP. This was related to the HTC process that alters the structure of the hydrochar by degrading hemicellulose and cellulose, which makes the HY require less energy during the first stage of pyrolysis while increasing lignin content that provides thermal stability and presents higher bond energy [78,79].

During combustion (Fig. 6), E_a slightly increased with α between 0.1 and 0.2 for all the samples because of the volatiles release and their combustion [80], then began to decrease as it continued into the second stage because the active char reacts continuously with the available oxygen and undergoes thermal cracking to form lower compounds [81]. During both the first and second stage of combustion, the average activation energy value of HY (116 and 47 kJ/mol respectively) remained lower than EGM (158 kJ/mol and 114 kJ/mol) and VP (149 kJ/mol and 103 kJ/mol). This remark highlighted that HY has a greater porous structure and higher surface area, which contribute to surface combustion reactions [61,78,80].

Li et al. [82], Kabakcı SB [80], Wilk et al. [83], and Santana et al. [84] have also observed similar phenomena. Their studies revealed that the HTC treatment reduced the activation energies necessary for the pyrolysis of cedarwood sawdust and wood sawdust, as well as the combustion of acacia and coffee beans. Interestingly, contrasting results were obtained in the pyrolysis kinetic studies of corn cobs [62] and coconut shell waste [85], as well as the combustion kinetic studies of wood sawdust [80] and agricultural waste [16] (Table 3). In these cases, the activation energies for hydrochars were found to increase. Therefore, it appears that the HTC treatment may not have a favorable impact on the subsequent pyrolysis and combustion processes of these biomass materials, as it could potentially raise the activation energy requirement [86].

3.3.2. Pre-exponential factor

The energy compensation effect method was used to estimate the values of A. Table S8 and Table S9 list the values of A during pyrolysis and combustion at each conversion rate calculated according to Eq. (8), where the values of the activation energy used came from the STK method since no significative variations of E_a values were highlighted between the *iso*-conversional methods. The corresponding plots are given in Figure S5 and Figure S6. The high coefficients of determination ($R^2 > 0.99$) demonstrate the applicability of ECE, which is the linear correlation between $E_{a,i}$, and $\ln[A_i]$. During the first stage of pyrolysis, the overall pre-exponential values of HY were lower than those of EGM and VP, remaining prettily constant with α in the order of $10^5 – 10^6$ s^{-1}. However, a slight variance of A with α was revealed in the second stage for EGM and HY, indicating more complex chemical reactions. The pre-exponential factors of EGM and HY increased from an order of 10^{13} and 10^7 s^{-1} up to 10^{18} and 10^{13} s^{-1} at a conversion rate of 0.8 and 0.6, respectively, then decreased to 10^{14} and 10^6 s^{-1} at $\alpha = 0.9$. A higher pre-exponential value implicates an increased frequency of molecular collisions, thereby necessitating a greater amount of heat transfer [87]. Furthermore, while values of A less than 10^9 s^{-1} typically indicate poor reactivity related mainly to surface reactions, or tight complex if not dependant on the surface area, A values greater than 10^9 s^{-1} represent simple complex inbound reactions, which demand larger activation energies [88,89].

During the first stage of combustion, the pre-exponential values of HY showed a small increase of A from 10^9 to 10^{11} s^{-1} between $\alpha = 0.1$ and 0.2, then decreased up to 10^4 s^{-1} at $\alpha = 0.9$. In the second stage, all

Table 3
Estimated activation energies of the pyrolysis and combustion of the raw and the HTC-treated feedstocks from previous studies.

Sample	HTC conditions	E_a	Reference
Pyrolysis			
Cedarwood sawdust		80.8	[82]
Cedarwood sawdust Hydrochar	240 °C – 10 min	55.3	[82]
Corn Cobs		46.0	[62]
Corn Cobs Hydrochar	230 °C – 60 min	70.4	[62]
Wood sawdust		162.8	[80]
Wood sawdust Hydrochar	220 °C – 90 min	153.1	[80]
Coconut shell waste		194.5	[85]
Coconut shell waste Hydrochar	200 °C – 30 min	221.9	[85]
Combustion			
Acacia		99.8	[83]
Acacia Hydrochar	200 °C – 240 min	95.8	[83]
Agricultural waste		86.2	[16]
Agricultural waste Hydrochar	240 °C – 60 min	99.5	[16]
Wood sawdust		152.4	[80]
Wood sawdust Hydrochar	220 °C – 90 min	171.7	[80]
Coffee beans		138.7	[84]
Coffee beans Hydrochar	250 °C – 40 min	132.4	[84]

the samples provided a pre-exponential value $\leq 10^9\ s^{-1}$, decreasing from 10^1 and $10^{-1}\ s^{-1}$, from 10^9 to $10^1\ s^{-1}$, and from 10^7 to $10^3\ s^{-1}$, respectively for HY, EGM, and VP. Generally, A values below $10^4\ s^{-1}$, are primarily associated with the combustion of porous carbon characterized by a lower E_a value [90]. These findings suggest that a broad range of pre-exponential values implies a more complex composition of the sample, requiring multiple energy levels at different conversion degrees during the combustion process [78,87].

3.3.3. Reaction mechanism

The kinetic mechanism function was determined by using the master-plot method based on the activation energy from the STK method. According to Eq. (11), the best fit between the experimental and theoretical curves of the master plot revealed the most appropriate reaction model. The results are displayed in Figure S7 and Figure S8. Different reaction mechanisms were identified for each step of pyrolysis and combustion of HY, EGM, and VP. During the first stage of pyrolysis, HY and EGM are dominated by the one-dimensional diffusion–reaction mechanism (D1), migrating respectively to the reaction order model F4 and F6 in the second stage. This was mostly ascribed to the ongoing release of volatiles and the creation of more porous structures, which improved the diffusion mechanism [91]. Instead, VP was characterized by reaction order model F3, thus was assumed that the rate of reaction was mainly proportional to the concentration of the reactants. Also, during the first and second stages of combustion of EGM and VP the experimental master plot revealed the best fit with the theoretical curves of the reaction order model F3 – F1 and F2 – F1, respectively. However, HY was best described with the two-dimensional diffusion mechanism (D2) in the first stage, approaching the second-order geometrical contraction model (R2) in the second stage. This behavior suggests that after volatile release, combustion processes began at the outside of the char particles and moved inside toward the central core. This model assumed that the reaction rate was controlled by the decomposition occurring on the surface, thus resulting in the contraction of area [89,92].

Combining the reaction model with Eq. (3), the kinetic equations describing the pyrolysis and combustion of HY, EGM, and VP can be obtained, as reported in Table 4 and Table 5.

3.3.4. Thermodynamic parameters

By replacing the corresponding value of E_a obtained from the STK method (Table S2 and Table S5) in the Equations (12) – (14), the value of Gibbs free energy, ΔG, change of enthalpy, ΔH, and change of entropy, ΔS, were obtained. The corresponding values at each conversion degree for both the pyrolysis and combustion are listed in Table S10 and Table S11, while a graphical representation is displayed in Fig. 7 and Fig. 8. Enthalpy is the total energy consumed by biomass samples during pyrolysis or combustion reactions predicting the bond strength [61]. The results demonstrate a similar shifting pattern between the change of ΔH and E_a for all the samples during both pyrolysis and combustion. Moreover, the positive values of ΔH revealed that pyrolysis and combustion of HY, EGM, and VP were based on endothermic reactions, meaning that molecules absorbed heat energy to break and establish new chemical bonds [93]. Also, the average difference between E_a and ΔH, for each material and in both the case of pyrolysis and combustion, was less than 6 kJ/mol, meaning that HY, EGM, and VP are prone to reaction since the potential energy barrier is low [87].

Table 4
Pyrolysis rate equations of HY, EGM, and VP at 10 °C/min.

Sample	Reaction rate equation	Stage [°C]
HY	$\frac{d\alpha}{dt} = 1.97\times10^{6}e^{-(82.19/RT)}0.5\alpha$	114 – 310
	$\frac{d\alpha}{dt} = 9.68\times10^{12}e^{-(160.19/RT)}(1-\alpha)^{4}$	310 – 728
EGM	$\frac{d\alpha}{dt} = 2.53\times10^{15}e^{-(170.93/RT)}0.5\alpha$	154 – 291
	$\frac{d\alpha}{dt} = 2.07\times10^{17}e^{-(197.50/RT)}(1-\alpha)^{6}$	291 – 649
VP	$\frac{d\alpha}{dt} = 2.30\times10^{12}e^{-(155.66/RT)}(1-\alpha)^{3}$	123 – 657

Table 5
Combustion rate equations of HY, EGM, and VP at 10 °C/min.

Sample	Reaction rate equation	Stage [°C]
HY	$\frac{d\alpha}{dt} = 8.28\times10^{10}e^{-(115.92/RT)}[-ln(1-\alpha)]^{-1}$	135 – 374
	$\frac{d\alpha}{dt} = 12.41e^{-(47.08/RT)}2(1-\alpha)^{1/2}$	374 – 830
EGM	$\frac{d\alpha}{dt} = 1.33\times10^{13}e^{-(158.61/RT)}(1-\alpha)^{3}$	157 – 377
	$\frac{d\alpha}{dt} = 2.59\times10^{9}e^{-(114.02/RT)}(1-\alpha)$	377 – 708
VP	$\frac{d\alpha}{dt} = 6.92\times10^{11}e^{-(149.27/RT)}(1-\alpha)^{2}$	156 – 377
	$\frac{d\alpha}{dt} = 6.73\times10^{6}e^{-(103.51/RT)}(1-\alpha)$	377 – 650

The Gibbs free energy provides information about the spontaneity and direction of reactions. Higher values of ΔG imply lower favorability of the reactions [61]. Overall, HY showed a lower average value of ΔG compared with EGM and VP in both the case of pyrolysis and combustion, meaning that the reactions of HY's precursors require an input of more energy.

The ΔS value reflects the degree of disorder in a system. The higher ΔS, the less the system is near to its own thermodynamic equilibrium, demonstrating more reactivity [65]. The lower value of ΔS for HY indicates that the hydrochar is more structurally ordered compared to the original biomasses. This could be the result of the removal of volatile components and the restructuring of carbonaceous materials after HTC, leading to a more stable and structured product.

Considering all available data, including kinetic and thermodynamic characteristics, as well as combustion and pyrolysis indexes, might be inferred that the hydrochar achieved a more thermodynamically stable, structurally ordered, and energetically favorable state through the co-HTC process, thus resulting in a potentially valuable product.

4. Conclusions

This study contributes novel data and understanding on the unique properties and conversion kinetics of winemaking waste-derived hydrochar. This expansion of the knowledge base is an important step towards the valorization of winemaking waste streams and the development of a circular bioeconomy.

Thermogravimetric analysis of pyrolysis and combustion highlighted that potentially co-HTC might reduce unstable biomass compounds, i.e. hemicellulose and cellulose, while increasing those with higher bond energy such as lignin. Also, modifying the resulting hydrochar's structure promotes its thermal stability and might grant a less turbulent combustion process, expressed by the reduced devolatilization and combustion index compared to the raw biomasses. Interestingly, the hydrochar from co-HTC of VP and EGM exhibited reduced activation energy for both pyrolysis and combustion processes. The diffusion–reaction mechanism dominated the pyrolysis' first stage of HY and EGM, while the reaction order model controlled both their second stage and that of the VP. Also, during combustion, stages I and II of EGM and VP were regulated by the reaction order model, however, HY by the diffusion model in the first stage and the geometrical contraction model in the second stage. Lastly, the analysis of thermodynamic parameters suggests that HY achieved a more stable thermodynamic state and favorable energy characteristics through the co-HTC process. These outcomes highlight the potential value of HY from HTC of winery and distillery by-products as a solid biofuel and provide practical utility in terms of designing and optimizing large-scale reactors. Also, they contribute to the efficient and economically viable development of

Fig. 7. Trend of thermodynamic parameters of HY, EGM, and VP during pyrolysis.

industrial processes, as well as support the advancement of biomass waste valorization and the transition towards more sustainable energy systems.

CRediT authorship contribution statement

Alessandro Cardarelli: Writing – original draft, Visualization, Validation, Methodology, Formal analysis, Data curation, Conceptualization. **Marco Barbanera:** Writing – review & editing, Visualization, Supervision, Resources, Conceptualization.

Declaration of competing interest

The authors declare that they have no known competing financial

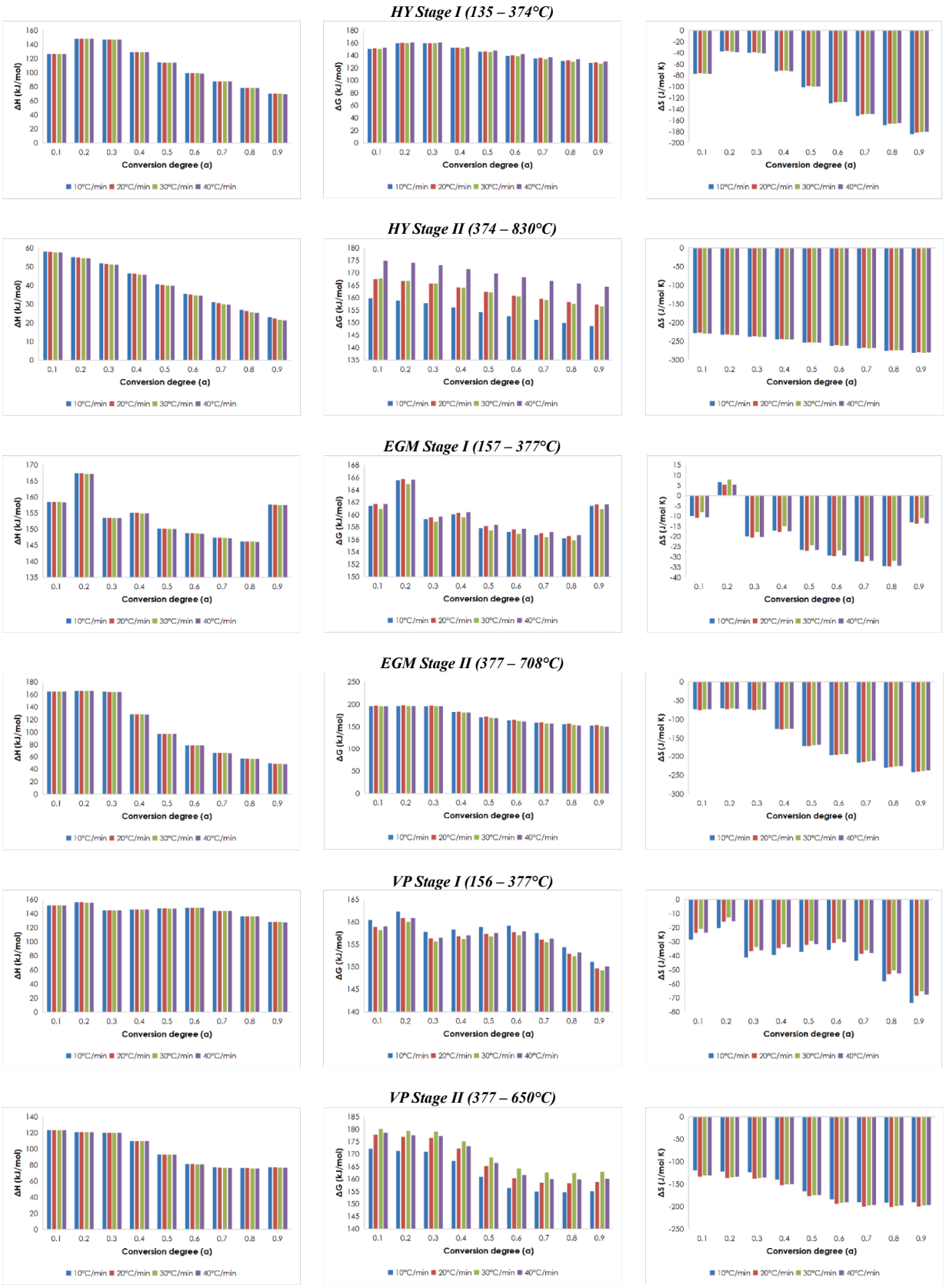

Fig. 8. Trend of thermodynamic parameters of HY, EGM, and VP during combustion.

interests or personal relationships that could have appeared to influence the work reported in this paper.

Data availability

Data will be made available on request.

Acknowledgements

The research was supported by the Project "Network 4 Energy Sustainable Transition—NEST", Project code PE0000021, funded under the National Recovery and Resilience Plan (NRRP), Mission 4, Component 2, Investment 1.3 — Call for tender No. 1561 of 11.10.2022 of Ministero dell'Universita`e della Ricerca (MUR); funded by the European Union—NextGenerationEU.

Appendix A. Supplementary data

Supplementary data to this article can be found online at https://doi.org/10.1016/j.fuel.2024.132256.

References

[1] Eurostat. Sustainable development in the European Union: monitoring report on progress towards the SDGs in an EU context, edition 6th edition 2022 Publications Office of the European Union Luxembourg 2022.
[2] European Commission. European Green Deal: EU agrees stronger legislation to accelerate the rollout of renewable energy 2023;https://ec.europa.eu/commission/presscorner/detail/en/IP_23_2061.
[3] Directive (EU) 2023/2413. Directive (EU) 2023/2413 of the European Parliament and of the Council of 18 October 2023 on the promotion of energy from renewable sources. 2023;http://data.europa.eu/eli/dir/2023/2413/oj.
[4] Eurostat. Share of renewable energy in gross final energy consumption by sector. 2023;https://ec.europa.eu/eurostat/databrowser/product/view/nrg_ind_ren.
[5] European Environment Agency (EEA). Trends and projections in Europe 2022 - EEA Report No 10/2022 2022.
[6] European Environment Agency (EEA). Share of energy consumption from renewable sources in Europe - 8th EAP 2023;https://www.eea.europa.eu/en/analysis/indicators/share-of-energy-consumption-from.
[7] International Organisation of Vine and Wine (OIV). Annual Assessment of the World Vine and Wine Sector in 2022 2022;https://www.oiv.int/.
[8] Dwyer K, Hosseinian F, Rod M. The Market Potential of Grape Waste Alternatives. J Food Res 2014;3(2):91. https://doi.org/10.5539/jfr.v3n2p91.
[9] Nerantzis ET, Panagiotis T. Integrated enology-utilization of winery by-products into high added value products. J Sci Technol 2006;1(3):79–89.
[10] Rodríguez LA, Toro ME, Vazquez F, Correa-Daneri ML, Gouiric SC, Vallejo MD. Bioethanol production from grape and sugar beet pomaces by solid-state fermentation. Int J Hydrogen Energy 2010;35:5914–7. https://doi.org/10.1016/j.ijhydene.2009.12.112.
[11] Muhlack RA, Potumarthi R, Jeffery DW. Sustainable wineries through waste valorisation: A review of grape marc utilisation for value-added products. Waste Manag 2018;72:99–118. https://doi.org/10.1016/j.wasman.2017.11.011.
[12] Tena M, Luque B, Perez M, Solera R. Enhanced hydrogen production from sewage sludge by cofermentation with wine vinasse. Int J Hydrogen Energy 2020;45:15977–84. https://doi.org/10.1016/j.ijhydene.2020.04.075.
[13] Sharma HB, Sarmah AK, Dubey B. Hydrothermal carbonization of renewable waste biomass for solid biofuel production: A discussion on process mechanism, the influence of process parameters, environmental performance and fuel properties of hydrochar. Renew Sustain Energy Rev 2020;123:109761. https://doi.org/10.1016/j.rser.2020.109761.
[14] Cavali M, Libardi Junior N, De Sena JD, Woiciechowski AL, Soccol CR, Belli Filho P, et al. A review on hydrothermal carbonization of potential biomass wastes, characterization and environmental applications of hydrochar, and biorefinery perspectives of the process. Sci Total Environ 2023;857:159627. https://doi.org/10.1016/j.scitotenv.2022.159627.
[15] Zhu S, Preuss N, You F. Advancing sustainable development goals with machine learning and optimization for wet waste biomass to renewable energy conversion. J Clean Prod 2023;422:138606. https://doi.org/10.1016/j.jclepro.2023.138606.
[16] Wu S, Wang Q, Cui D, Sun H, Yin H, Xu F, et al. Evaluation of fuel properties and combustion behaviour of hydrochar derived from hydrothermal carbonisation of agricultural wastes. J Energy Inst 2023;108:101209. https://doi.org/10.1016/j.joei.2023.101209.
[17] Roslan SZ, Zainudin SF, Mohd Aris A, Chin KB, Musa M, Mohamad Daud AR, et al. Hydrothermal Carbonization of Sewage Sludge into Solid Biofuel: Influences of Process Conditions on the Energetic Properties of Hydrochar. Energies 2023;16:2483. https://doi.org/10.3390/en16052483.
[18] Barbanera M, Cardarelli A, Carota E, Castellini M, Giannoni T, Ubertini S. Valorization of winery and distillery by-products by hydrothermal carbonization. Sci Rep 2021;11:23973. https://doi.org/10.1038/s41598-021-03501-7.
[19] Prasongthum N, Suemanotham A, Sisuthog W, Thanmongkhon Y, Chaiya C, Attanatho L. Hydrothermal carbonization of oil palm trunk: Hydrochar properties and combustion behaviors. Energy Rep 2023;9:380–6. https://doi.org/10.1016/j.egyr.2023.09.033.
[20] Sattasathuchana S, Parnthong J, Youngian S, Faungnawakij K, Rangsunvigit P, Kitiyanan B, et al. Energy efficiency of bio-coal derived from hydrothermal carbonized biomass: Assessment as sustainable solid fuel for municipal biopower plant. Appl Therm Eng 2023;221:119789. https://doi.org/10.1016/j.applthermaleng.2022.119789.
[21] Yu Y, Guo Y, Wang G, El-Kassaby YA, Sokhansanj S. Hydrothermal carbonization of waste ginkgo leaf residues for solid biofuel production: Hydrochar characterization and its pelletization. Fuel 2022;324:124341. https://doi.org/10.1016/j.fuel.2022.124341.
[22] Wu S, Wang Q, Cui D, Wang X, Wu D, Bai J, et al. Analysis of fuel properties of hydrochar derived from food waste and biomass: Evaluating varied mixing techniques pre/post-hydrothermal carbonization. J Clean Prod 2023;430:139660. https://doi.org/10.1016/j.jclepro.2023.139660.
[23] Cardarelli A, Barbanera M. Substitution of Fossil Coal with Hydrochar from Agricultural Waste in the Electric Arc Furnace Steel Industry: A Comprehensive Life Cycle Analysis. Energies 2023;16:5686. https://doi.org/10.3390/en16155686.
[24] Rammohan D, Kishore N, Uppaluri RVS. Insights on kinetic triplets and thermodynamic analysis of Delonix regia biomass pyrolysis. Bioresour Technol 2022;358:127375. https://doi.org/10.1016/j.biortech.2022.127375.
[25] Liu Y, Song Y, Fu J, Ao W, Ali Siyal A, Zhou C, et al. Co-pyrolysis of sewage sludge and lignocellulosic biomass: Synergistic effects on products characteristics and kinetics. Energ Conver Manage 2022;268:116061. https://doi.org/10.1016/j.enconman.2022.116061.
[26] Kumar M, Shukla SK, Upadhyay SN, Mishra PK. Analysis of thermal degradation of banana (Musa balbisiana) trunk biomass waste using iso-conversional models. Bioresour Technol 2020;310:123393. https://doi.org/10.1016/j.biortech.2020.123393.
[27] Wu S, Wang Q, Fang M, Wu D, Cui D, Pan S, et al. Hydrothermal carbonization of food waste for sustainable biofuel production: Advancements, challenges, and future prospects. Sci Total Environ 2023;897:165327. https://doi.org/10.1016/j.scitotenv.2023.165327.
[28] Garcia Torrent J, Fernandez Anez N, Medic Pejic L, Montenegro ML. Assessment of self-ignition risks of solid biofuels by thermal analysis. Fuel 2015;143:484–91. https://doi.org/10.1016/j.fuel.2014.11.074.
[29] Starink MJ. The determination of activation energy from linear heating rate experiments: a comparison of the accuracy of isoconversion methods. Thermochim Acta 2003;404:163–76. https://doi.org/10.1016/S0040-6031(03)00144-8.
[30] Akahira T, Sunose T. Method of determining activation deterioration constant of electrical insulating materials. Res Report Chiba Inst Technol (Sci Technol) 1971;16:22–31.
[31] Ozawa T. A New Method of Analyzing Thermogravimetric Data. BCSJ 1965;38:1881–6. https://doi.org/10.1246/bcsj.38.1881.
[32] Flynn JH, Wall LA. A quick, direct method for the determination of activation energy from thermogravimetric data. J Polym Sci B Polym Lett 1966;4:323–8. https://doi.org/10.1002/pol.1966.110040504.
[33] Vyazovkin S, Burnham AK, Criado JM, Pérez-Maqueda LA, Popescu C, Sbirrazzuoli N. ICTAC Kinetics Committee recommendations for performing kinetic computations on thermal analysis data. Thermochim Acta 2011;520:1–19. https://doi.org/10.1016/j.tca.2011.03.034.
[34] Mumbach GD, Alves JLF, Da Silva JCG, Di Domenico M, De Sena RF, Marangoni C, et al. Pyrolysis of cocoa shell and its bioenergy potential: evaluating the kinetic triplet, thermodynamic parameters, and evolved gas analysis using TGA-FTIR. Biomass Conv Bioref 2022;12:723–39. https://doi.org/10.1007/s13399-020-01058-5.
[35] Doyle CD. Kinetic analysis of thermogravimetric data. J Appl Polym Sci 1961;5:285–92. https://doi.org/10.1002/app.1961.070051506.
[36] Vyazovkin S, Burnham AK, Favergeon L, Koga N, Moukhina E, Pérez-Maqueda LA, et al. ICTAC Kinetics Committee recommendations for analysis of multi-step kinetics. Thermochim Acta 2020;689:178597. https://doi.org/10.1016/j.tca.2020.178597.
[37] Liu H, Xiang C, Mu J, Yao J, Ye D, Jin K, et al. Thermodynamic model and kinetic compensation effect of oil sludge pyrolysis based on thermogravimetric analysis. Therm Sci 2022;26:259–72. https://doi.org/10.2298/TSCI200926350L.
[38] Azizi K, Moshfegh Haghighi A, Keshavarz Moraveji M, Olazar M, Lopez G. Co-pyrolysis of binary and ternary mixtures of microalgae, wood and waste tires through TGA. Renew Energy 2019;142:264–71. https://doi.org/10.1016/j.renene.2019.04.116.
[39] Singh S, Patil T, Tekade SP, Gawande MB, Sawarkar AN. Studies on individual pyrolysis and co-pyrolysis of corn cob and polyethylene: Thermal degradation behavior, possible synergism, kinetics, and thermodynamic analysis. Sci Total Environ 2021;783:147004. https://doi.org/10.1016/j.scitotenv.2021.147004.
[40] Doyle CD. Estimating isothermal life from thermogravimetric data. J Appl Polym Sci 1962;6:639–42. https://doi.org/10.1002/app.1962.070062406.
[41] Alves JLF, Da Silva JCG, Da Silva Filho VF, Alves RF, Ahmad MS, Ahmad MS, et al. Bioenergy potential of red macroalgae Gelidium floridanum by pyrolysis: Evaluation of kinetic triplet and thermodynamics parameters. Bioresour Technol 2019;291:121892. https://doi.org/10.1016/j.biortech.2019.121892.
[42] Cardarelli A, Pinzi S, Barbanera M. Effect of torrefaction temperature on spent coffee grounds thermal behaviour and kinetics. Renew Energy 2022;185:704–16. https://doi.org/10.1016/j.renene.2021.12.116.

[43] Wang S, Dai G, Yang H, Luo Z. Lignocellulosic biomass pyrolysis mechanism: A state-of-the-art review. Prog Energy Combust Sci 2017;62:33–86. https://doi.org/10.1016/j.pecs.2017.05.004.
[44] Libra JA, Ro KS, Kammann C, Funke A, Berge ND, Neubauer Y, et al. Hydrothermal carbonization of biomass residuals: a comparative review of the chemistry, processes and applications of wet and dry pyrolysis. Biofuels 2011;2:71–106. https://doi.org/10.4155/bfs.10.81.
[45] Islam MA, Asif M, Hameed BH. Pyrolysis kinetics of raw and hydrothermally carbonized Karanj (Pongamia pinnata) fruit hulls via thermogravimetric analysis. Bioresour Technol 2015;179:227–33. https://doi.org/10.1016/j.biortech.2014.11.115.
[46] Mäkelä M, Kwong CW, Broström M, Yoshikawa K. Hydrothermal treatment of grape marc for solid fuel applications. Energ Conver Manage 2017;145:371–7. https://doi.org/10.1016/j.enconman.2017.05.015.
[47] Pala M, Kantarli IC, Buyukisik HB, Yanik J. Hydrothermal carbonization and torrefaction of grape pomace: A comparative evaluation. Bioresour Technol 2014;161:255–62. https://doi.org/10.1016/j.biortech.2014.03.052.
[48] Volpe M, Fiori L. From olive waste to solid biofuel through hydrothermal carbonisation: The role of temperature and solid load on secondary char formation and hydrochar energy properties. J Anal Appl Pyrol 2017;124:63–72. https://doi.org/10.1016/j.jaap.2017.02.022.
[49] Mastral AM, Murillo R, Callén MS, García T, Snape CE. Influence of Process Variables on Oils from Tire Pyrolysis and Hydropyrolysis in a Swept Fixed Bed Reactor. Energy Fuels 2000;14:739–44. https://doi.org/10.1021/ef990183e.
[50] Mishra A, Nanda S, Ranjan Parida M, Jena PK, Dwibedi SK, Manjari Samantaray S, et al. A comparative study on pyrolysis kinetics and thermodynamic parameters of little millet and sunflower stems biomass using thermogravimetric analysis. Bioresour Technol 2023;367:128231. https://doi.org/10.1016/j.biortech.2022.128231.
[51] Sakhiya AK, Anand A, Vijay VK, Kaushal P. Thermal decomposition of rice straw from rice basin of India to improve energy-pollution nexus: Kinetic modeling and thermodynamic analysis. Energy Nexus 2021;4:100026. https://doi.org/10.1016/j.nexus.2021.100026.
[52] Lei Z, Wang S, Fu H, Gao W, Wang B, Zeng J, et al. Thermal pyrolysis characteristics and kinetics of hemicellulose isolated from Camellia Oleifera Shell. Bioresour Technol 2019;282:228–35. https://doi.org/10.1016/j.biortech.2019.02.131.
[53] Kim S-S, Ly HV, Kim J, Choi JH, Woo HC. Thermogravimetric characteristics and pyrolysis kinetics of Alga Sagarssum sp. biomass. Bioresour Technol 2013;139:242–8. https://doi.org/10.1016/j.biortech.2013.03.192.
[54] Li Y, Liu H, Xiao K, Jin M, Xiao H, Yao H. Combustion and Pyrolysis Characteristics of Hydrochar Prepared by Hydrothermal Carbonization of Typical Food Waste: Influence of Carbohydrates, Proteins, and Lipids. Energy Fuels 2020;34:430–9. https://doi.org/10.1021/acs.energyfuels.9b02940.
[55] He Q, Ding L, Gong Y, Li W, Wei J, Yu G. Effect of torrefaction on pinewood pyrolysis kinetics and thermal behavior using thermogravimetric analysis. Bioresour Technol 2019;280:104–11. https://doi.org/10.1016/j.biortech.2019.01.138.
[56] He Q, Cheng C, Raheem A, Ding L, Shiung Lam S, Yu G. Effect of hydrothermal carbonization on woody biomass: From structure to reactivity. Fuel 2022;330:125586. https://doi.org/10.1016/j.fuel.2022.125586.
[57] Yu Y, Lau A, Sokhansanj S. Hydrothermal carbonization and pelletization of moistened wheat straw. Renew Energy 2022;190:1018–28. https://doi.org/10.1016/j.renene.2022.03.152.
[58] Cárdenas-Aguiar E, Gascó G, Paz-Ferreiro J, Méndez A. Thermogravimetric analysis and carbon stability of chars produced from slow pyrolysis and hydrothermal carbonization of manure waste. J Anal Appl Pyrol 2019;140:434–43. https://doi.org/10.1016/j.jaap.2019.04.026.
[59] Mortari DA, Perondi D, Rossi GB, Bonato JL, Godinho M, Pereira FM. The influence of water-soluble inorganic matter on combustion of grape pomace and its chars produced by slow and fast pyrolysis. Fuel 2021;284:118880. https://doi.org/10.1016/j.fuel.2020.118880.
[60] Cao W, Li J, Martí-Rosselló T, Zhang X. Experimental study on the ignition characteristics of cellulose, hemicellulose, lignin and their mixtures. J Energy Inst 2019;92:1303–12. https://doi.org/10.1016/j.joei.2018.10.004.
[61] Lang Q, Zhang B, Liu Z, Chen Z, Xia Y, Li D, et al. Co-hydrothermal carbonization of corn stalk and swine manure: Combustion behavior of hydrochar by thermogravimetric analysis. Bioresour Technol 2019;271:75–83. https://doi.org/10.1016/j.biortech.2018.09.100.
[62] Zhang T, Kang K, Nanda S, Dalai AK, Xie T, Zhao Y. Comparative study on fuel characteristics and pyrolysis kinetics of corn residue-based hydrochar produced via microwave hydrothermal carbonization. Chemosphere 2022;291:132787. https://doi.org/10.1016/j.chemosphere.2021.132787.
[63] Ebrahim Malool M, Keshavarz Moraveji M, Shayegan J. Co-hydrothermal carbonization of digested sewage sludge and sugarcane bagasse: Integrated approach for waste management, optimized production, characterization and Pb (II) adsorption. Alex Eng J 2023;74:79–105. https://doi.org/10.1016/j.aej.2023.05.018.
[64] Zhuang X, Zhan H, Huang Y, Song Y, Yin X, Wu C. Conversion of industrial biowastes to clean solid fuels via hydrothermal carbonization (HTC): Upgrading mechanism in relation to coalification process and combustion behavior. Bioresour Technol 2018;267:17–29. https://doi.org/10.1016/j.biortech.2018.07.002.
[65] Ma J, Luo H, Li Y, Liu Z, Li D, Gai C, et al. Pyrolysis kinetics and thermodynamic parameters of the hydrochars derived from co-hydrothermal carbonization of sawdust and sewage sludge using thermogravimetric analysis. Bioresour Technol 2019;282:133–41. https://doi.org/10.1016/j.biortech.2019.03.007.
[66] Ferreira AF, Ribau JP, Costa M. A decision support method for biochars characterization from carbonization of grape pomace. Biomass Bioenergy 2021;145:105946. https://doi.org/10.1016/j.biombioe.2020.105946.
[67] Niu Y, Tan H, Hui S. Ash-related issues during biomass combustion: Alkali-induced slagging, silicate melt-induced slagging (ash fusion), agglomeration, corrosion, ash utilization, and related countermeasures. Prog Energy Combust Sci 2016;52:1–61. https://doi.org/10.1016/j.pecs.2015.09.003.
[68] Vamvuka D, Sfakiotakis S. Combustion behaviour of biomass fuels and their blends with lignite. Thermochim Acta 2011;526:192–9. https://doi.org/10.1016/j.tca.2011.09.021.
[69] Xu Z-X, Song H, Zhang S, Tong S-Q, He Z-X, Wang Q, et al. Co-hydrothermal carbonization of digested sewage sludge and cow dung biogas residue: Investigation of the reaction characteristics. Energy 2019;187:115972. https://doi.org/10.1016/j.energy.2019.115972.
[70] Chen X, Ma X, Peng X, Lin Y, Yao Z. Conversion of sweet potato waste to solid fuel via hydrothermal carbonization. Bioresour Technol 2018;249:900–7. https://doi.org/10.1016/j.biortech.2017.10.096.
[71] Parshetti GK, Quek A, Betha R, Balasubramanian R. TGA–FTIR investigation of co-combustion characteristics of blends of hydrothermally carbonized oil palm biomass (EFB) and coal. Fuel Process Technol 2014;118:228–34. https://doi.org/10.1016/j.fuproc.2013.09.010.
[72] Alves JLF, Da Silva JCG, Mumbach GD, Domenico MD, De Sena RF, Machado RAF, et al. Demonstrating the Suitability of Tamarind Residues to Bioenergy Exploitation Via Combustion Through Physicochemical Properties, Performance Indexes, and Emission Characteristics. Bioenerg Res 2020;13:1308–20. https://doi.org/10.1007/s12155-020-10158-z.
[73] Riva L, Cardarelli A, Andersen GJ, Buø TV, Barbanera M, Bartocci P, et al. On the self-heating behavior of upgraded biochar pellets blended with pyrolysis oil: Effects of process parameters. Fuel 2020;278:118395. https://doi.org/10.1016/j.fuel.2020.118395.
[74] Cardarelli A, De Santis M, Cirilli F, Barbanera M. Computational fluid dynamics analysis of biochar combustion in a simulated ironmaking electric arc furnace. Fuel 2022;328:125267. https://doi.org/10.1016/j.fuel.2022.125267.
[75] Lu Y, Yang H, Karasev AV, Wang C, Jönsson PG. Applications of Hydrochar and Charcoal in the Iron and Steelmaking Industry—Part 1: Characterization of Carbonaceous Materials. Sustainability 2022;14:9488. https://doi.org/10.3390/su14159488.
[76] Huang X, Ng KW, Giroux L, Duchesne M, Li D, Todoschuk T. Interaction Behavior of Biogenic Material with Electric Arc Furnace Slag. Fuels 2021;2:420–36. https://doi.org/10.3390/fuels2040024.
[77] Lopez-Velazquez MA, Santes V, Balmaseda J, Torres-Garcia E. Pyrolysis of orange waste: A thermo-kinetic study. J Anal Appl Pyrol 2013;99:170–7. https://doi.org/10.1016/j.jaap.2012.09.016.
[78] Lang Q, Liu Z, Li Y, Xu J, Li J, Liu B, et al. Combustion characteristics, kinetic and thermodynamic analyses of hydrochars derived from hydrothermal carbonization of cattle manure. J Environ Chem Eng 2022;10:106938. https://doi.org/10.1016/j.jece.2021.106938.
[79] Dong X, Guo S, Ma M, Zheng H, Gao X, Wang S, et al. Hydrothermal carbonization of millet stalk and dilute-acid-impregnated millet stalk: combustion behaviors of hydrochars by thermogravimetric analysis and a novel mixed-function fitting method. Fuel 2020;273:117734. https://doi.org/10.1016/j.fuel.2020.117734.
[80] Kabakcı SB. Pyrolysis and combustion characteristics and kinetics of wood sawdust and wood sawdust hydrochar. Environ Prog Sustainable. Energy 2020:39. https://doi.org/10.1002/ep.13315.
[81] Tariq R, Mohd Zaifullizan Y, Salema AA, Abdulatif A, Ken LS. Co-pyrolysis and co-combustion of orange peel and biomass blends: Kinetics, thermodynamic, and ANN application. Renew Energy 2022;198:399–414. https://doi.org/10.1016/j.renene.2022.08.049.
[82] Li H, Wang S, Yuan X, Xi Y, Huang Z, Tan M, et al. The effects of temperature and color value on hydrochars' properties in hydrothermal carbonization. Bioresour Technol 2018;249:574–81. https://doi.org/10.1016/j.biortech.2017.10.046.
[83] Wilk M, Magdziarz A, Jayaraman K, Szymańska-Chargot M, Gökalp I. Hydrothermal carbonization characteristics of sewage sludge and lignocellulosic biomass. A comparative study Biomass and Bioenergy 2019;120:166–75. https://doi.org/10.1016/j.biombioe.2018.11.016.
[84] Santos Santana M, Pereira Alves R, Da Silva Borges WM, Francisquini E, Guerreiro MC. Hydrochar production from defective coffee beans by hydrothermal carbonization. Bioresour Technol 2020;300:122653. https://doi.org/10.1016/j.biortech.2019.122653.
[85] Cheng C, Guo Q, Ding L, Gong Y, Yu G. Insights into pyrolysis process of coconut shell waste hydrochar: In-situ structural evolution and reaction kinetics. J Clean Prod 2024;448:141701. https://doi.org/10.1016/j.jclepro.2024.141701.
[86] Wang S, Wen Y, Shi Z, Niedzwiecki L, Baranowski M, Czerep M, et al. Effect of hydrothermal carbonization pretreatment on the pyrolysis behavior of the digestate of agricultural waste: A view on kinetics and thermodynamics. Chem Eng J 2022;431:133881. https://doi.org/10.1016/j.cej.2021.133881.
[87] Chong CT, Mong GR, Ng J-H, Chong WWF, Ani FN, Lam SS, et al. Pyrolysis characteristics and kinetic studies of horse manure using thermogravimetric analysis. Energ Conver Manage 2019;180:1260–7. https://doi.org/10.1016/j.enconman.2018.11.071.
[88] Turmanova SC, Genieva SD, Dimitrova AS, Vlaev LT. Non-isothermal degradation kinetics of filled with rise husk ash polypropene composites. Express Polym Lett 2008;2:133–46. https://doi.org/10.3144/expresspolymlett.2008.18.
[89] Thejaswini N, Annapureddy PKR, Rammohan D, Kishore N. Kinetics and thermodynamics of non-isothermal pyrolysis of *Terminalia chebula* branches at

different heating rates. Int J of Chemical Kinetics 2023;55:673–87. https://doi.org/10.1002/kin.21677.
[90] Barbanera M, Cotana F, Di Matteo U. Co-combustion performance and kinetic study of solid digestate with gasification biochar. Renew Energy 2018;121:597–605. https://doi.org/10.1016/j.renene.2018.01.076.
[91] El-Sayed SA, Mostafa ME. Pyrolysis and co-pyrolysis of Egyptian olive pomace, sawdust, and their blends: Thermal decomposition, kinetics, synergistic effect, and thermodynamic analysis. J Clean Prod 2023;401:136772. https://doi.org/10.1016/j.jclepro.2023.136772.
[92] Zhang J, Zou H, Liu J, Evrendilek F, Xie W, He Y, et al. Comparative (co-)pyrolytic performances and by-products of textile dyeing sludge and cattle manure: Deeper insights from Py-GC/MS, TG-FTIR, 2D-COS and PCA analyses. J Hazard Mater 2021;401:123276. https://doi.org/10.1016/j.jhazmat.2020.123276.
[93] Boubacar Laougé Z, Merdun H. Pyrolysis and combustion kinetics of Sida cordifolia L. using thermogravimetric analysis. Bioresour Technol 2020;299:122602. https://doi.org/10.1016/j.biortech.2019.122602.